Topological supercurrents interaction and fluctuations in the multiterminal Josephson effect

Hong-Yi Xie^{1,2} and Alex Levchenko¹

¹Department of Physics, University of Wisconsin–Madison, Madison, Wisconsin 53706, USA ²Kavli Institute of Theoretical Sciences, University of the Chinese Academy of Sciences, Beijing 100190, China



(Received 23 December 2018; revised manuscript received 11 March 2019; published 26 March 2019)

We study the Josephson effect in the multiterminal junction of topological superconductors. We use the symmetry-constrained scattering matrix approach to derive band dispersions of emergent subgap Andreev bound states in a multidimensional parameter space of superconducting phase differences. We find distinct topologically protected band crossings that serve as monopoles of finite Berry curvature. Particularly, in a four-terminal junction the admixture of 2π and 4π periodic levels leads to the appearance of finite-energy Majorana-Weyl nodes. This topological regime in the junction can be characterized by a quantized nonlocal conductance that measures the Chern number of the corresponding bands. In addition, we calculate current-phase relations, variance, and cross correlations of topological supercurrents in multiterminal contacts and discuss the universality of these transport characteristics. At the technical level these results are obtained by integrating over the group of a circular ensemble that describes the scattering matrix of the junction. We briefly discuss our results in the context of observed fluctuations of the gate dependence of the critical current in topological planar Josephson junctions and comment on the possibility of parity measurements from the switching current distributions in multiterminal Majorana junctions.

DOI: 10.1103/PhysRevB.99.094519

I. INTRODUCTION

The universality of conductance fluctuations (UCF) is the hallmark of mesoscopic physics [1–4]. This phenomenon emerges from the quantum coherence of electron trajectories and is sensitive to changes in external magnetic field or gate voltage. At temperatures below the Thouless energy, $T < E_{Th}$, which is related to the inverse dwell time for an electron to diffuse across the sample $E_{\rm Th} = D/L^2$, the rms value of conductance fluctuations saturates to the universal value of the order conductance quantum $\sim e^2/h$ as long as the characteristic sample size L is smaller than the dephasing length $L < L_{\phi}$. Interaction effects in normal metals barely change the magnitude and universality of conductance fluctuations, although they are crucially important in determining the temperature dependence of dephasing effects and, in particular, L_{ϕ} [5]. The robustness of UCF can be rooted to the random matrix theory description of Wigner-Dyson statistics of electron energy levels in disordered conductors [6]. Indeed, in the Landauer picture of transport across a mesoscopic sample, conductance is given by e^2/h times the number of single-particle levels within the energy strip of the width of Thouless energy. While the average number of such levels depends on the dimensionality, random matrix theory predicts that their fluctuation is universally of the order of one [7,8].

When superconductivity is induced at the boundary of the mesoscopic sample via the proximity effect, the universality of fluctuations remains intact [9,10]. Indeed, the magnitude of sample-to-sample conductance fluctuations changes only by a numerical factor of the order of unity whose value depends on the underlying symmetry [11,12]. Interestingly, the universality of fluctuations extends beyond conductance as it also manifests in the Josephson current of a

superconducting-normal-superconducting (SNS) bridge. Indeed, extending the original ideas of Al'tshuler and Spivak [13], who argued that random shifts of subgap energy levels with superconducting phase difference would alter the current, Beenakker showed [14] that in short junctions, $L \ll \xi$, where ξ is the superconducting coherence length, the rms value of critical current fluctuations saturates to a universal bound $\sim e\Delta/h$ determined only by the superconducting energy gap Δ in the leads. Further a complete characterization of the supercurrent variance as a function of phase across the point contact Josephson junction was computed by Chalker and Macêdo [15]. In long junctions, $L \gg \xi$, supercurrent fluctuations cease to be universal and scale with $\sim eE_{Th}/h$. However, a remarkable property of these fluctuations is that there is a regime where the entire critical current through the junction can be determined by the mesoscopic contribution when the average current is suppressed.

In recent years the interest in Josephson physics has shifted towards junctions whose elements include topological materials [16–24] or where topological properties are enabled by a specific design of the hybrid junction with otherwise conventional materials [25–29]. These possibilities and advances motivate our work to investigate how universal mesoscopic effects manifest in topological Josephson junctions that, in particular, host Majorana states (see the review in [30] and references therein). We carry out this analysis in the context of multiterminal devices that were brought into the spotlight of recent theoretical attention with the observation that they can emulate topological matter [31–39], which triggered experimental efforts in realizing these systems in various proximitized circuits [40–44].

The rest of the paper is organized as follows. In Sec. II we briefly review symmetry-constrained scattering matrix

transport formalism in application to the Josephson effect in multiterminal circuits. In Sec. III we apply these methods to two-terminal junctions as a benchmark and then extend our analysis to three- and four-terminal devices, for which we compute the emergent band structure of subgap states, investigate their topology, and derive transport characteristics such as transconductance and supercurrent. In Sec. IV we focus our attention on the statistical properties of topological supercurrents and obtain analytical results for variance that takes a universal form and also inherits the 4π periodicity of the Majorana Josephson effect.

II. SCATTERING MATRIX FORMALISM

Consider a Josephson junction (JJ) where n superconducting (S) terminals are connected through the common normal (N) region, thus forming a multiterminal SNS contact. To keep the presentation simple, we assume that each superconducting lead is coupled by only a single conducting channel in the normal region and both time-reversal and chiral symmetries are broken (unconventional classes D and C [30]). Formation of the subgap bound states in the JJs is the result of coherent Andreev reflections that describe electron-to-hole conversion at the superconductor-normal interface. In n-terminal junctions an elastic scattering event at energy ε is characterized by a scattering matrix $\hat{S}(\varepsilon) \in U(2n)$, where 2 denotes the particle-hole degrees of freedom. In what follows we assume that all leads have the same superconducting gap Δ and normalize all energies in units of Δ . The particle-hole (PH) symmetry is represented by

$$\hat{S}(\varepsilon) = \mathcal{P}\hat{S}(-\varepsilon)\mathcal{P}^{-1},\tag{1}$$

where the antiunitary PH transform \mathcal{P} falls into two categories, $\mathcal{P}^2=\pm 1$. For example, for s-wave paring, $\mathcal{P}=\hat{\tau}_1\mathcal{K}$ ($\mathcal{P}^2=+1$) in the spin-nondegenerate case, and $\mathcal{P}=i\hat{\tau}_2\mathcal{K}$ ($\mathcal{P}^2=-1$) in the spin-degenerate case, where $\hat{\tau}_{1,2,3}$ are the Pauli matrices acting in particle-hole space and \mathcal{K} denotes the complex conjugation. The Andreev bound-state energies are determined by the determinant equation [14]

$$Det[\mathbb{I}_{2n} - \hat{R}_A(\varepsilon, \hat{\theta})\hat{S}_N(\varepsilon)] = 0.$$
 (2)

Here $\hat{S}_N(\varepsilon)$ is the scattering matrix of the normal region, and $\hat{R}_A(\varepsilon, \hat{\theta})$ is the scattering matrix describing Andreev reflections, where $\theta_{\alpha} \in \{\theta_0, \theta_1, \dots, \theta_{n-1}\}$ is the diagonal matrix of superconducting phases. We set $\theta_0 = 0$ owing to global gauge invariance. Due to the PH symmetry equation (1) these scattering matrices take the block-diagonal forms

$$\hat{S}_{N}(\varepsilon) = \begin{bmatrix} \hat{s}(\varepsilon) & 0\\ 0 & \hat{s}^{*}(-\varepsilon) \end{bmatrix},$$

$$\hat{R}_{A}(\varepsilon, \hat{\theta}) = e^{-i\arccos\varepsilon} \begin{bmatrix} 0 & e^{i\hat{\theta}}\\ -\mathcal{P}^{2}e^{-i\hat{\theta}} & 0 \end{bmatrix},$$
(3)

where $\hat{s}(\varepsilon) \in \mathrm{U}(n)$. The determinant in Eq. (2) simplifies further to a degree-n characteristic polynomial of $\gamma(\varepsilon) \equiv e^{-2i\arccos\varepsilon}$,

$$P_n(\gamma; \hat{\theta}, \varepsilon) \equiv \text{Det}[\mathbb{I}_n + \mathcal{P}^2 \gamma(\varepsilon) e^{i\hat{\theta}} s^*(-\varepsilon) e^{-i\hat{\theta}} s(\varepsilon)], \quad (4)$$

which is (anti)palindromic $\mathcal{P}^{2n}\gamma^n P_n(\gamma^{-1}) = P_n(\gamma)$. Importantly, from Eq. (4) we observe that, for a fixed normal-region

scattering matrix \hat{s} , the Andreev bands of $\mathcal{P}^2 = \pm 1$ symmetry classes are dual via the relation

$$\varepsilon_{\mathcal{P}^2-+1}^2(\hat{\theta}) + \varepsilon_{\mathcal{P}^2--1}^2(\hat{\theta}) = 1. \tag{5}$$

Previously, we extensively discussed the $\mathcal{P}^2=-1$ scenario in application to three- and four-terminal junctions [34,35]. In this work we primarily focus on the Andreev spectrum of $\mathcal{P}^2=+1$ junctions that can support zero-energy Majorana modes. In what follows, we also assume energy-independent scattering matrices \hat{s} that correspond to, for example, weak links where the length of the junction is small compared to the superconducting coherence length, $L\ll\xi$, so that retardation effects of traveling quasiparticles can be neglected. We note that the existence of Majorana zero modes does not depend on this assumption.

To study the energy spectra of emergent states in junctions with $\mathcal{P}^2 = +1$ terminals, we introduce the scattering matrix at $\varepsilon = 0$.

$$\hat{S}_0 \equiv \hat{R}_A(0, \hat{\theta}) \hat{S}_N = i \begin{bmatrix} 0 & -e^{i\hat{\theta}} \hat{s}^* \\ e^{-i\hat{\theta}} \hat{s} & 0 \end{bmatrix}, \tag{6}$$

which belongs to the circular real ensemble since $\text{Det}\hat{S}_0 = (-1)^n$. Via Eq. (2) the zero-energy Majorana modes are determined by the determinant equation of an antisymmetric matrix $\hat{m}(\theta)$,

$$Det[\hat{m}(\hat{\theta})] = 0, \quad \hat{m}(\hat{\theta}) = e^{-i\hat{\theta}/2} \hat{s} e^{i\hat{\theta}/2} - e^{i\hat{\theta}/2} \hat{s}^T e^{-i\hat{\theta}/2}. \quad (7)$$

From here we draw important properties. (i) For $n \in \text{odd}$, Eq. (7) is generally satisfied for any scattering matrices \hat{s} and phases $\hat{\theta}$. This implies that Andreev-Majorana zero modes are present at any phases and robust to elastic scattering and superconducting order parameter nonuniformity. These nondispersive flat bands do not contribute to Josephson currents. (ii) For $n \in \text{even}$, the Andreev bands cross at zero energy at phases determined by the Pfaffian equation

$$Pf_{n \in \text{even}}[\hat{m}(\hat{\theta})] = 0. \tag{8}$$

Based on our study of two- and four-terminal junctions, we conjecture that there always exists a pair of Majorana zero modes on an (n-2)-dimensional hypersurface in the $\theta = (\theta_1, \ldots, \theta_{n-1})$ space described by Eq. (8). Next, we reveal the energy spectrum of the junction for several concrete forms of the scattering matrix.

III. MULTITERMINAL JOSEPHSON EFFECT

A. Two-terminal junctions

We first study two-terminal junctions as a benchmark. We parametrize the 2×2 unitary matrix \hat{s} by four independent parameters,

$$s = \begin{bmatrix} \sqrt{1 - T}e^{i\varphi_{00}} & \sqrt{T}e^{i\varphi_{01}} \\ \sqrt{T}e^{i\varphi_{10}} & -\sqrt{1 - T}e^{i(\varphi_{01} + \varphi_{10} - \varphi_{00})} \end{bmatrix}, \tag{9}$$

where $T \in [0, 1]$, representing the normal-region transmission and scattering phases $\varphi_{00,01,10} \in [0, 2\pi]$. The subgap spectrum of excitations is determined by the n=2 characteristic polynomial (4) via the equation $P_2(\gamma) = \gamma^2 + 2B_2\gamma + 1 = 0$, where the B_2 function takes the form $B_2(\theta) = 1 - 1$

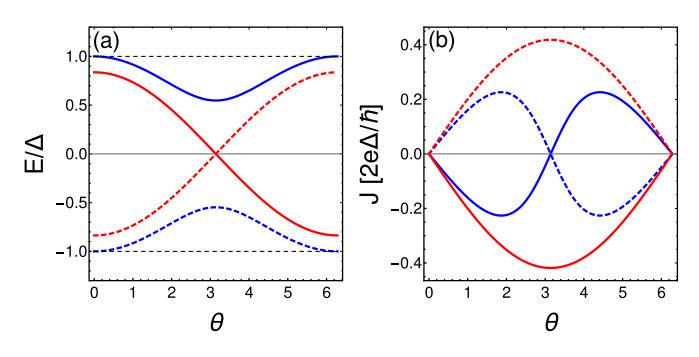


FIG. 1. (a) Energy spectrum [Eq. (10)] and (b) Josephson current [Eq. (11)] for $\mathcal{P}^2=+1$ two-terminal topological Josephson junctions. We take T=0.7 and $\phi=\pi$. The red (blue) curves are the results for topologically nontrivial leads $\mathcal{P}^2=+1$ (topologically trivial leads $\mathcal{P}^2=-1$). In (a) the black dashed lines indicate the continuum edge $\varepsilon=E/\Delta=1$.

 $2T \sin^2(\vartheta/2)$, with $\vartheta \equiv \theta - \phi + \pi$ and $\phi \equiv \varphi_{10} - \varphi_{01}$. The two branches of dispersive solutions are given by

$$\varepsilon(\vartheta) = \pm \begin{cases} \sqrt{T}\cos(\vartheta/2), & \mathcal{P}^2 = +1, \\ \sqrt{1 - T\sin^2(\vartheta/2)}, & \mathcal{P}^2 = -1, \end{cases}$$
(10)

where for comparison we recall the results for the conventional $\mathcal{P}^2 = -1$ junctions. For finite transmission $T \neq 0$, the n=2 Pfaffian equation (8) reduces to $\mathrm{Pf}_2(\theta) = m_{01} \sim \cos(\vartheta/2) = 0$, so that a Majorana crossing occurs at $\vartheta = (2k+1)\pi$, with $k \in \mathbb{Z}$. The zero-temperature Josephson current $J(\theta) \equiv (2e\Delta/\hbar)\partial_\theta \varepsilon$ takes the form

$$J(\vartheta) = \pm \frac{e\Delta}{\hbar} \times \begin{cases} \sqrt{T} \sin(\vartheta/2), & \mathcal{P}^2 = +1, \\ T \sin \vartheta/4\varepsilon(\vartheta), & \mathcal{P}^2 = -1. \end{cases}$$
(11)

The typical energy dispersion and supercurrent-phase relation are shown in Fig. 1. We note that for $\phi=\pi$ doubly degenerate Majorana states emerge at $\theta=\pi$, and the energy and supercurrent exhibit 4π periodicity in θ . In addition, the bound states are detached from the continuum with a minimal gap $1-\sqrt{T}$ at $\theta=0$ and 2π . Equations (10) and (11) are consistent with the prior results (e.g., Ref. [45]).

B. Three-terminal junctions

For n=3 the spectrum of localized states is determined by the palindromic polynomial $P_3(\gamma) = (\gamma + 1)(\gamma^2 + 2B_3\gamma + 1) = 0$ and composed of three bands,

$$\varepsilon_{\pm}(\boldsymbol{\theta}) = \pm \sqrt{\frac{1 - B_3(\boldsymbol{\theta})}{2}}, \quad \varepsilon_0(\boldsymbol{\theta}) = 0.$$
 (12)

Adopting the same parametrization of the scattering matrix as in Ref. [34], the B_3 function can be found in the closed analytical form

$$B_3 = \frac{1}{2} \left[2a^2 - (1+a^2)(b^2+c^2-2b^2c^2) - 4abc\sqrt{(1-b^2)(1-c^2)}\cos\varphi \right]$$

$$+ bc(1-a^2)\cos\vartheta_1 + (1-a^2)\sqrt{(1-b^2)(1-c^2)}\cos\vartheta_2$$

$$+ \left[bc(1+a^2)\sqrt{(1-b^2)(1-c^2)} \right]$$

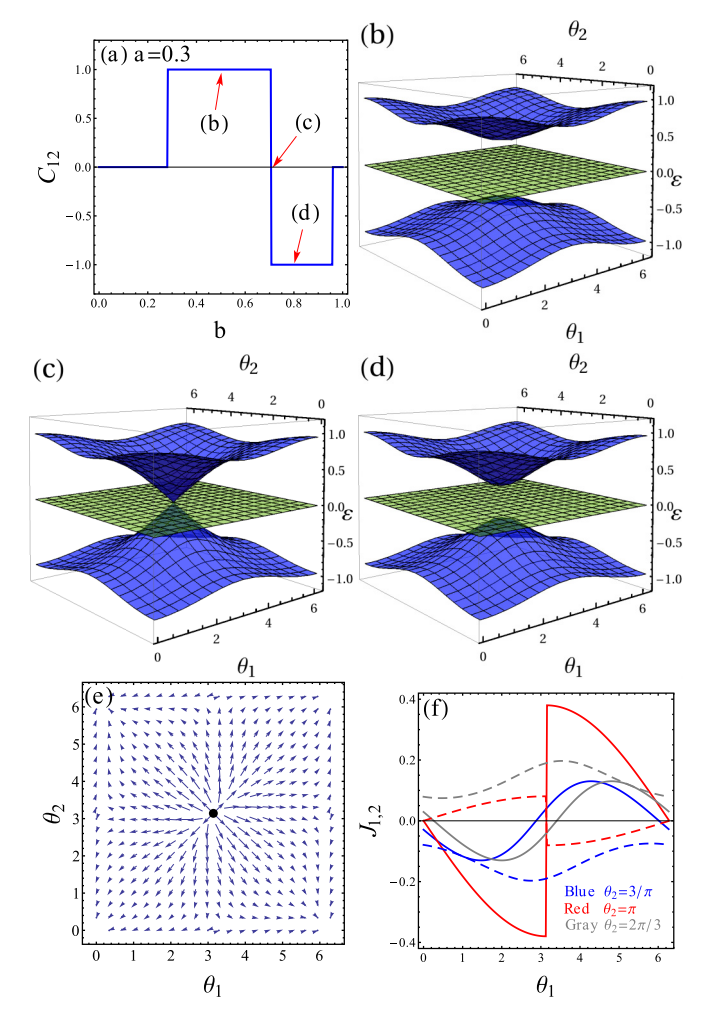


FIG. 2. Energy spectrum and Josephson current for $\mathcal{P}^2=1$ three-terminal junctions. We take $c=\sqrt{1-b^2}$, a=0.3, and $\varphi=\phi_1=\phi_2=\pi$. (a) Chern number as a function of b. (b)–(d) Andreev spectra at b=0.5, $b_0=1/\sqrt{2}$, and 0.8. (e) and (f) Josephson currents $J_{1,2}$ as functions of $\theta_{1,2}$ at $b=b_0$. (e) Hedgehoglike pattern of the current flow about the Weyl node. (f) $J_{1,2}$ as a function of θ_1 for various values of θ_2 .

$$+ a(b^2 + c^2 - 2b^2c^2)\cos\varphi \Big]$$

$$\times \cos(\vartheta_1 - \vartheta_2) + a(b^2 - c^2)\sin\varphi\sin(\vartheta_1 - \vartheta_2). \tag{13}$$

Consequently, there are only six independent parameters of the scattering matrix $\{a, b, c, \varphi, \phi_{1,2}\}$ that enter the spectrum of Andreev bound states. Furthermore, scattering phases $\phi_{1,2}$ only shift the phases of the leads $\vartheta_{1,2} = \theta_{1,2} - \phi_{1,2}$.

Depending on the choice of scattering matrix parameters, we find rich behavior of the energy bands. For the special case $c=\sqrt{1-b^2}$ and $\phi=\pi$ the spectrum exhibits nontrivial topology, as shown in Fig. 2. Zero-energy Weyl points appear at $\vartheta_{1,2}=0$ for $b=b_0=1/\sqrt{2}$ [Figs. 2(b)–2(d)]. As shown in Fig. 2(a), the Chern number of the corresponding band structure exhibits a sign jump $C_{12}=\mathrm{sgn}(b_0-b)$ for $b\to b_0$. We also note that the other topological phase transitions for $b\approx 0.28$ and 0.96 are related to the gap closing/reopening at the Andreev band edge $\varepsilon=1$. Figure 2(e) displays Josephson currents $J_{1,2}$ in two terminals when the system is tuned to the

nodal gapless states. In Fig. 2(f) the series of one-dimensional cuts in either the θ_1 phase or θ_2 shows how Josephson currents change as one tunes phases to the vicinity of nodal points. We observe that moving across the node, currents exhibit discontinuous jumps. Note that the Majorana flat band $\varepsilon_0=0$ does not contribute to the Josephson current.

C. Four-terminal junctions

The energy spectrum of four-terminal junctions can host Majorana zero modes and Weyl nodes simultaneously. The four Andreev bands determined by the palindromic equation $P_4(\gamma) = \gamma^4 + A_4\gamma^3 + B_4\gamma^2 + A_4\gamma + 1 = 0$ are given explicitly by the following expressions:

$$\varepsilon(\theta) = \pm \sqrt{\frac{4 - A_4 \pm \sqrt{A_4^2 - 4B_4 + 8}}{8}},\tag{14}$$

where the A_4 and B_4 functions are defined by

$$A_{4} = \mathsf{A}_{0} + 2 \sum_{j>0} \operatorname{Re}[\mathsf{A}_{j}e^{-i\theta_{j}}] + 2 \sum_{0 < j < k} \operatorname{Re}[\mathsf{A}_{jk}e^{-i\theta_{jk}}],$$

$$B_{4} = \mathsf{B}_{0} + 2 \sum_{j>0} \operatorname{Re}[\mathsf{B}_{j}e^{-i\theta_{j}}] + 2 \sum_{0 < j < k} \operatorname{Re}[\mathsf{B}_{jk}e^{-i\theta_{jk}}]$$

$$+ 2 \sum_{jkl \in P_{123}} \operatorname{Re}[\mathsf{B}_{jkl}e^{-i\theta_{jkl}}]. \tag{15}$$

Here we have used shorthand notations for phases $\theta_{jk} \equiv \theta_j - \theta_k$ and $\theta_{jkl} \equiv \theta_j + \theta_k - \theta_l$, permutations $P_{123} \in \{123, 312, 231\}$, and Re[·] denotes the real part of a complex number. Additionally, parameters **A** and **B** are functions of the scattering matrix elements $\{s_{jk}\}$. Specifically,

$$\mathsf{A}_0 = \sum_{j=0}^{3} |s_{jj}|^2, \quad \mathsf{A}_j = s_{0j}^* s_{j0}, \quad \mathsf{A}_{jk} = s_{kj}^* s_{jk}, \tag{16}$$

and

$$B_{0} = \sum_{j < k} |s_{jj;kk}|^{2}, \quad B_{j} = \sum_{k \neq 0, j} s_{0k;kj}^{*} s_{jk;k0},$$

$$B_{jk} = \sum_{l \neq i, k} s_{kl;lj}^{*} s_{jl;lk}, \quad B_{jkl} = s_{0k;lj}^{*} s_{k0;jl}, \quad (17)$$

with $s_{jk;lq} \equiv s_{jk}s_{lq} - s_{jq}s_{lk}$. The scattering matrix is parametrized by 16 real parameters as in Ref. [46], where $\{a, b, c, d, h, f\} \in [0, 1]$ and $\varphi_{00,11,01,10,02,20,03,30,12,21} \in [0, 2\pi]$. An inspection of these expressions reveals that despite the fact that we need ten independent phases to parametrize the scattering matrix, only six effective angles, $\phi_1 \equiv \varphi_{12} - \varphi_{21}$, $\phi_2 \equiv \varphi_{13} - \varphi_{31}$, $\phi_3 \equiv \varphi_{14} - \varphi_{41}$, $\phi_4 \equiv \varphi_{22} - \varphi_{23}$, $\phi_5 \equiv \varphi_{22} - \varphi_{32}$, and $\phi_6 \equiv \varphi_{11} + \varphi_{22} - \varphi_{12} - \varphi_{21}$, affect the Andreev spectrum in Eq. (14). The zero-energy states are determined by the n = 4 Pfaffian equation (8),

$$Pf_4(\boldsymbol{\theta}) = \sum_{jkl \in P_{123}} \left[s_{0k;lj} e^{i\theta_{jkl}/2} + s_{jl;k0} e^{-i\theta_{jkl}/2} \right] = 0.$$
 (18)

Via the unitary condition of \hat{s} , Eq. (18) implies that $\sum_{jkl \in P_{123}} C_{jkl} \cos[(\theta_{jkl} - \zeta_{jkl})/2] = 0$, where C_{ijk} and ζ_{ijk} are real functions of $\{s_{jk}\}$. Most importantly, this determines a

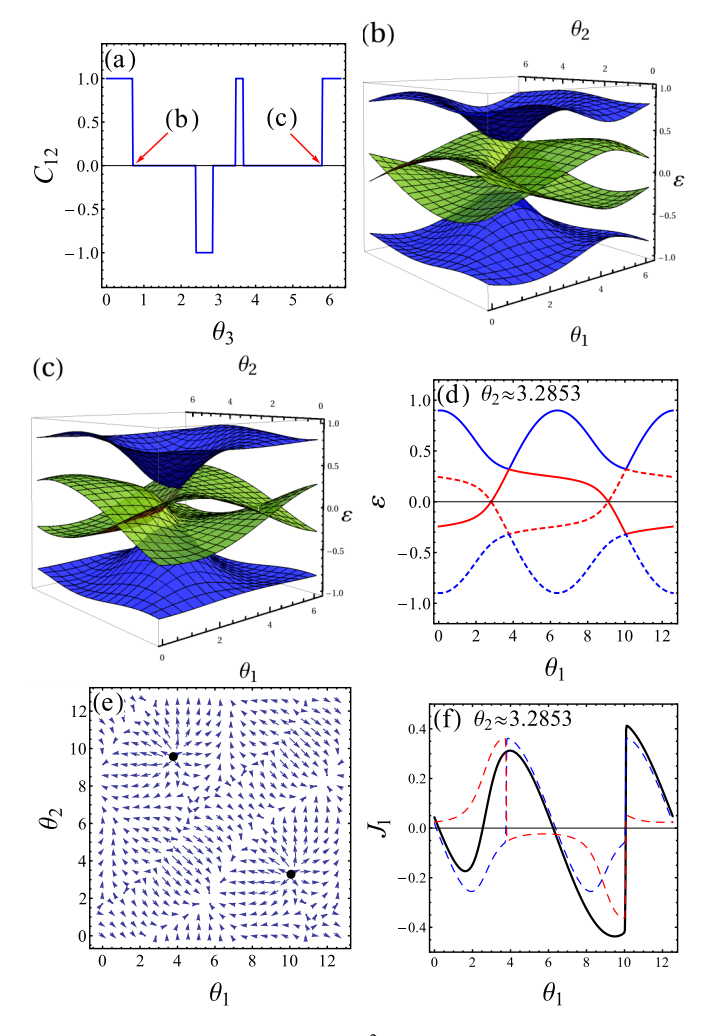


FIG. 3. Energy spectrum for $\mathcal{P}^2=1$ time-reversal-broken four-terminal junctions. The scattering matrix parameters are defined as in Ref. [34]. We take a=1/4, $b=1/\sqrt{3}$, c=1/5, d=1/2, f=1/3, h=4/5, $\phi_1=\phi_2=\pi$, $\phi_3=0$, $\phi_4=\phi_5=-\pi/3$, and $\phi_6=\pi/6$. (a) Chern number as a function of θ_3 . At $\theta_3^*\approx 0.6990$ and 5.7883, finite-energy Weyl nodes form at $(\theta_1^*,\theta_2^*)\approx (3.7785,3.2853)$ and (3.2046,3.0051), and the spectra are shown in (b) and (c), respectively. (d) Traces of the spectrum in (b) at $\theta_2=\theta_2^*$. Upper (blue) and lower (red) Andreev bands exhibit 2π and 4π periodicity, respectively. (e) The pattern of Josephson currents $J_{1,2}(\theta_1,\theta_2)$ corresponding to the spectrum in (b). The hedgehoglike singularities are present at the Weyl nodes $(\theta_1,\theta_2)\approx (\theta_1^*+2\pi,\theta_2^*)$ and $(\theta_1^*,\theta_2^*+2\pi)$. (f) Trace of $J_1(\theta_1)$ at $\theta_2=\theta_2^*$. The dashed lines denote the contributions of upper (blue) and lower (red) bands.

Majorana-crossing surface in θ space given by $\theta_{jkl} = \zeta_{jkl} \pm \frac{\pi}{2} \pmod{2\pi}$.

As a practical example, we study the energy bands of this model for the choice of incommensurate parameters: a=1/4, $b=1/\sqrt{3}$, c=1/5, d=1/2, f=1/3, h=4/5, $\phi_1=\phi_2=\pi$, $\phi_3=0$, $\phi_4=\phi_5=-\pi/3$, and $\phi_6=\pi/6$. The energy spectrum, corresponding Chern number, and Josephson currents are shown in Fig. 3. We observe that the lower bands exhibit 4π periodicity due to the Majorana crossings described by Eq. (18). Moreover, at $\theta_3=\theta_3^*\approx 0.6990$ [Fig. 3(b)] and 5.7883 [Fig. 3(c)] finite-energy Weyl nodes form at $(\theta_1^*,\theta_2^*)\approx$

(3.7785, 3.2853) and (3.2046,3.0051), respectively, between one of the higher and lower bands. The appearance of these nodal points is signaled by a change in the Chern number [Fig. 3(a)]. At this point we comment that it was recently shown that such Majorana-Weyl crossings occur in a different model of a four-terminal junction formed between the end states of one-dimensional topological superconductors (TSs) of class D [39]. It has been pointed out that a finite Chern number C_{ij} in this regime is associated with a quantized transconductance $G_{ij} = (2e^2/h)C_{ij}$. We confirm this result in our scattering matrix model and remark that the extra phase transitions in Fig. 3(a) are related to gap closing/reopening at the band edge $\varepsilon = 1$ that may not be stable since the higher bands can strongly hybridize with the continuum $\varepsilon > 1$.

The one-dimensional cut of the spectrum in Fig. 3(b) along θ_1 at $\theta_2 = \theta_2^* \approx 3.2853$ is shown in Fig. 3(d). The Josephson currents $J_{1,2}$ as functions of $\theta_{1,2}$ corresponding to the spectrum in Fig. 3(b) are shown in Fig. 3(e), where the hedgehoglike singularities are present at the Weyl nodes $(\theta_1^* + 2\pi, \theta_2^*)$ and $(\theta_1^*, \theta_2^* + 2\pi)$. We note that the other two nodal points at (θ_1^*, θ_2^*) and $(\theta_1^* + 2\pi, \theta_2^* + 2\pi)$ do not induce current singularities since the higher- and lower-band contributions cancel each other. This can be observed in Fig. 3(f), which displays $J_1(\theta_1)$ along the cut at $\theta_2 = \theta_2^*$.

IV. FLUCTUATIONS IN TOPOLOGICAL JUNCTIONS

In the previous section we studied Josephson current for the given realization of the scattering matrix. As alluded to in the Introduction, this current is expected to display reproducible sample-to-sample fluctuations, and it is thus of interest to study its statistical properties. We primarily focus on its variance and also on the cross-correlation function that can be experimentally accessed in the multiterminal devices. As is known from quantum transport theoretical approaches, statistical transport properties of phase-coherent mesoscopic systems can be conveniently computed by means of averaging over a random matrix that describes the system. In open systems, the averaging is done over the scattering matrix, and one typically considers two models of junctions: chaotic cavities or disordered contacts. The former case is more suitable for the model considered in this work. We thus follow classical works by Baranger and Mello [47] and Jalabert et al. [48], who studied conduction through a chaotic cavity on the assumption that the scattering matrix is uniformly distributed in the unitary group, restricted only by symmetry. This is the circular ensemble, introduced by Dyson and shown to apply to a chaotic cavity by Blumel and Smilansky [49]. In other words we consider a SNS junction where the normal region is a chaotic quantum dot [50].

The probability density $\rho(\vec{x})$, an invariant Haar measure, of the \hat{s} -matrix parameters \vec{x} is given by

$$\rho(\vec{x}) \equiv \sqrt{|\text{Det}\hat{M}(\vec{x})|}, \quad M_{\mu\nu} \equiv \sum_{i,j} \frac{\partial s_{ij}}{\partial x_{\mu}} \frac{\partial s_{ij}^*}{\partial x_{\nu}}.$$
 (19)

The distribution function of an observable $Q(\vec{x})$, defined as $P(Q) \equiv \int d\vec{x} \rho(\vec{x}) \delta[Q - Q(\vec{x})]$, is, in practice, calculated by

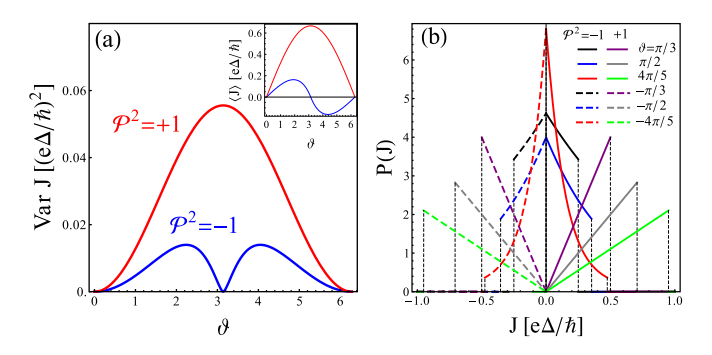


FIG. 4. Josephson current statistics of the two-terminal junctions. (a) Josephson current variance VarJ as a function of phase variable ϑ [Eq. (22)]. The inset shows the expectation value $\langle J \rangle$. (b) Probability distribution function P(J) for various phase variables ϑ [Eq. (23)].

the characteristic function

$$p(\lambda) = \langle e^{i\lambda Q(\bar{x})} \rangle, \quad P(Q) = \frac{1}{2\pi} \int d\lambda e^{-i\lambda Q} p(\lambda), \quad (20)$$

where $\langle \cdots \rangle \equiv \int d\vec{x} \rho(\vec{x})(\cdots)$, denoting the circular unitary ensemble (CUE) average.

For a benchmark we first study the statistics of the Josephson current $J(\vartheta)$ in the two-terminal junctions and take $2\Delta/\hbar$ as the units of J in the following discussion. From Eqs. (9) and (19) we obtain a constant invariant measure $\rho(T)=1$. We recall that this simplicity is specific to the unitary case; for instance, in orthogonal symmetry the probability density is not flat in T even for a single-channel limit. All the moments as well as the distribution function of the Josephson current can be obtained analytically. The m moment is given by the expression

$$\langle J^{m} \rangle = \frac{2}{m+2} \sin^{m} \left(\frac{\vartheta}{2} \right), \quad \mathcal{P}^{2} = +1,$$

$$\langle J^{m} \rangle = \frac{1}{m+1} \left(\frac{\sin \vartheta}{4} \right)^{m}$$

$$\times {}_{2}F_{1} \left[\frac{m}{2}, m+1; m+2; \sin^{2} \left(\frac{\vartheta}{2} \right) \right], \quad \mathcal{P}^{2} = -1,$$
(21b)

where $m \in \mathbb{N}$ and ${}_2F_1(a, b; c; z)$ is the hypergeometric function. Therefore, the variance for $\mathcal{P}^2 = +1$ reads

$$\operatorname{Var} J = \frac{1}{18} \sin^2 \left(\frac{\vartheta}{2}\right),\tag{22a}$$

whereas for the nontopological case $\mathcal{P}^2 = -1$ it has a different look,

$$\operatorname{Var} J = \frac{\sin^2 \vartheta}{192} \left[1 + \sin^2 \left(\frac{\vartheta}{2} \right) + \frac{113}{120} \sin^4 \left(\frac{\vartheta}{2} \right) + \cdots \right], \tag{22b}$$

as depicted in Fig. 4(a). In the topological regime the variance inherits 4π periodicity and has a remarkably simple form. In the nontopological regime, our result is similar to that of Chalker and Macêdo [15], albeit with different numeri-

cal coefficients as they considered the multimode disordered junction model, where averaging is done over the Dorokhov distribution of transmission eigenvalues. Finally, the Josephson current distribution function takes the form, for $\mathcal{P}^2 = +1$,

$$P(J; \vartheta) = \frac{2J}{J_c^+ |J_c^+|} \Theta(|J_c^+| - |2J - J_c^+|)$$
 (23a)

and, for $\mathcal{P}^2 = -1$,

$$P(J;\vartheta) = \frac{8\Theta(|J_c^-| - |2J - J_c^-|)}{|\sin\vartheta|K(J\tan\frac{\vartheta}{2})[1 + K^2(J\tan\frac{\vartheta}{2})]},$$
 (23b)

where $J_{\rm c}^+(\vartheta)=\sin(\vartheta/2)$ and $J_{\rm c}^-(\vartheta)=\sin(\vartheta/2)\,{\rm sgn}\, [\cos(\vartheta/2)]/2$ are the critical currents, $\Theta(x)$ is the Heaviside step function, and the function $K(x)=|x|+\sqrt{1+x^2}.$ As shown in Fig. 4(b), in both $\mathcal{P}^2=\pm 1$ classes the relation $P(J;-\vartheta)=P(-J;\vartheta)$ is satisfied. (i) For $\mathcal{P}^2=+1,\ P(J)$ is a linear function of J for which P(0)=0, and the slope is defined by the phase ϑ . In particular $P(J)=\delta(J)$ for $\vartheta=2k\pi$, with $k\in\mathbb{Z}.$ (ii) For $\mathcal{P}^2=-1,\ P(J)$ is smaller for a larger current amplitude, and $P(J)=\delta(J)$ for $\vartheta=k\pi$, with $k\in\mathbb{Z}.$

We proceed to study the Josephson current statistics of the three-terminal junctions. From Eq. (19) we obtain the probability density of the effective parameters $\vec{x} = (a, b, c, \varphi)$,

$$\rho(\vec{x}) = \mathcal{N}ab\sqrt{\frac{(2-a^2)[(1-a^2)(2-b^2) + a^2b^2\sin^2\varphi]}{(1-a^2)(1-b^2)(1-c^2)}},$$
(24)

where $\mathcal{N}\approx 1.7671\times 10^{-2}$ is the normalization constant. The numerical results of the expectation value, variance, and covariance of $J_{1,2}(\vartheta_{1,2})$ are shown in Fig. 5, where the covariance is defined as $\text{Cov}J_{1,2}\equiv \langle J_1J_2\rangle - \langle J_1\rangle\langle J_2\rangle$. The general relations $\langle J_1^m(\vartheta_1,\vartheta_2)\rangle = \langle J_2^m(\vartheta_2,\vartheta_1)\rangle$ and $\text{Cov}J_{1,2}(\vartheta_1,\vartheta_2)=\text{Cov}J_{1,2}(\vartheta_2,\vartheta_1)$ are satisfied. We observe that the variances and covariances distinguish the $\mathcal{P}^2=\pm 1$ junctions.

For $\mathcal{P}^2=+1$ three-terminal junctions, by integrating one and two terminals we can construct an effective two-terminal S-TS junction [51] which supports a single channel on one lead (topological), with phase $\theta_0=0$, and two channels on the other (conventional), with phase $\theta=\theta_1=\theta_2$. Defining $\vartheta=\vartheta_1$ and $\phi=\phi_2-\phi_1$ in Eqs. (12) and (13), we obtain the Josephson current through the two leads,

$$J(\vec{x}';\vartheta) = \frac{e\Delta}{\hbar} \frac{\partial_{\theta} B_3(\vartheta,\vartheta)}{4\varepsilon_{+}(\vartheta,\vartheta)},\tag{25}$$

which depends on five independent parameters, $\vec{x}' = (a,b,c,\varphi,\phi)$. We present the numerical results of the statistical properties of $J(\vartheta)$ for such a configuration in Fig. 6. The expectation and variance of J as functions of ϑ are shown in Fig. 6(a). The characteristic function $p(\lambda;\vartheta)$ for various ϑ is shown in Fig. 6(b). We observe that, for $\lambda\gg 1$, $p(\lambda)\propto \lambda^{-\alpha}$, with the exponent α being ϑ independent. We calculate the ϑ -averaged characteristic function $\bar{p}(\lambda)\equiv \frac{1}{2\pi}\int_0^{2\pi}d\vartheta\,p(\lambda;\vartheta)$ and fix the exponent $\alpha\sim 0.55$. In particular, this analysis enables us to extract the asymptotic behavior of the full distribution function P(J), which is found to exhibit a universal power-law scaling $P(J)\propto J^{-(1-\alpha)}$ in the limit $J\ll 1$.

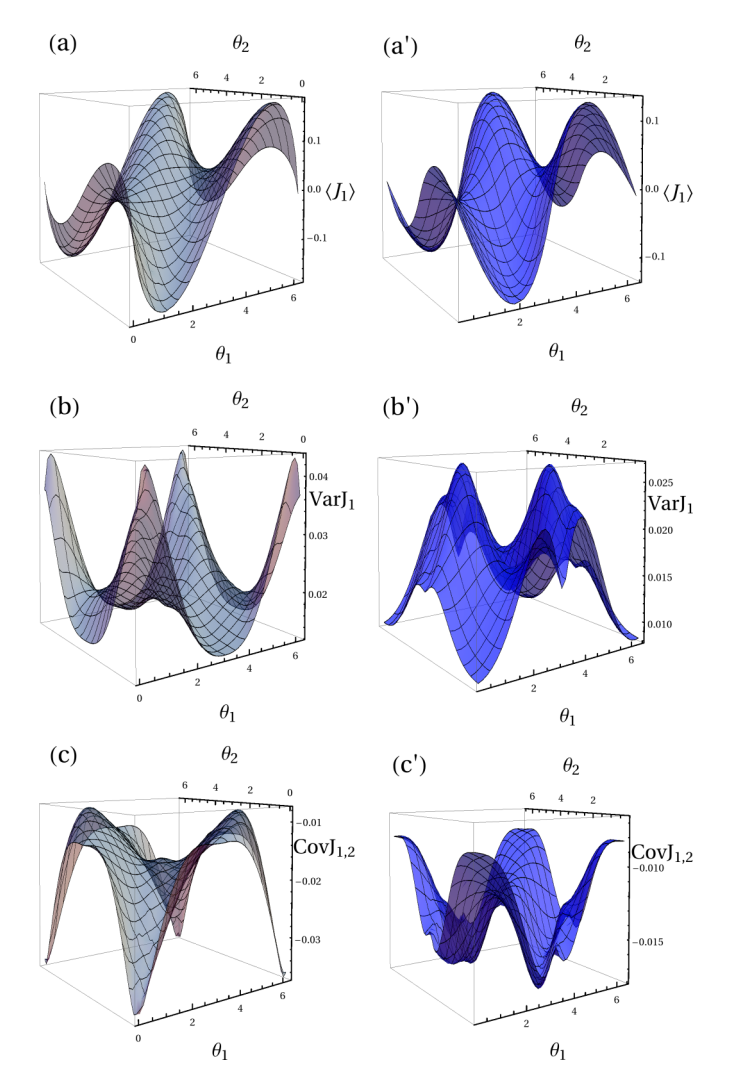


FIG. 5. Josephson current statistics of three-terminal junctions. The results for (a)–(c) $\mathcal{P}^2=+1$ and (a')–(c') $\mathcal{P}^2=-1$ junctions. (a) and (a') Expectation of J_1 as a function of $\vartheta_{1,2}$. (b) and (b') Variance of J_1 as a function of $\vartheta_{1,2}$. (c) and (c') Covariance of $J_{1,2}$ as a function of $\vartheta_{1,2}$.

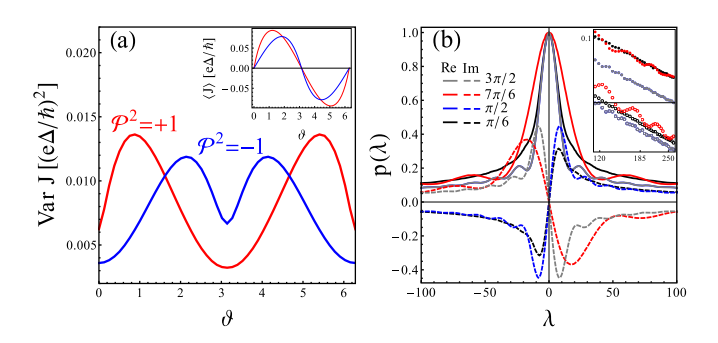


FIG. 6. Josephson current statistics of S-TS junctions. (a) Variance of J as a function of ϑ . We present the $\mathcal{P}^2=-1$ results for comparison. The inset shows the expectation value as a function of ϑ . (b) Characteristic function $p(\lambda)$ for various values of ϑ . The solid (dashed) lines are the real (imaginary) part of $p(\lambda)$. The inset is the log-log plot for $\lambda\gg 1$.

V. DISCUSSION AND OUTLOOK

In this work we applied methods of scattering matrix theory to study the transport properties of multiterminal Josephson junctions of topological superconductors. We have examined the spectrum of subgap states in two-, three-, and four-terminal configurations and determined that the texture of resulting Andreev bands in the multidimensional parameter space of superconducting phases can produce nonvanishing fluxes of the Berry curvature. These properties translate into the quantized nonlocal conductances of these devices. We have also studied the current-phase relationships and interaction of supercurrents, as well as their mesoscopic statistical properties. In particular, we discussed the universal regime of current fluctuations and computed supercurrent variance as well as the current cross-correlation function in the topological regime. We close this work with a few comments in relation to existing and possible future experiments in which the fundamental physics of multiterminal Josephsonic devices could be further explored.

Recently, Josephson supercurrent and conductance were measured as a function of geometry, temperature, and gate voltage in proximitized planar junction devices composed of superconductors and surface states of a topological insulator (S-TI-S junctions) in order to determine the nature of the electronic transport in these systems. The supercurrent was found to exhibit a sharp drop as a function of gate voltage (see Figs. 2 and 6 of Ref. [21]), superimposed with reproducible noise whose magnitude was a fraction of the critical current. The systematic trend in the critical current dependence was explained by a mechanism related to the relocation of the topological surface state with respect to trivial conducting two-dimensional states formed by band banding near the surface. In real space, a negative gating potential pushes the trivial state below the topological surface states, exposing the topological state to the disordered surface of the TI. As a result, the magnitude of the supercurrent changes sharply. The noise was attributed to the percolation effects as near the voltage threshold it is likely that local charge fluctuations cause the path of the supercurrent to be highly meandering. We wish to point out that there is possibly an alternative picture as this noise could be of mesoscopic origin. This evidence is further supported by observed similar reproducible noise features in Fraunhofer magneto-oscillations of the critical current. While our model is not directly applicable to S-TI-S junctions, we make the observation that the magnitude of current fluctuations is consistent with the expectation that disorder scattering causes observed mesoscopic effects.

In addition, we wish to note that related statistical properties of supercurrents can also be studied by measuring switching current distributions. In particular, for topological Josephson devices, the critical current measurements can potentially enable determining the parity state of a Majorana fermion (pair) in a junction since the supercurrent acquires an anomalous fractional component due to Majorana modes, $\pm \sin(\vartheta/2)$, where the sign encodes the parity. The typical switching measurement is performed by ramping the bias current through the junction to detect the current value at which the junction jumps to the finite voltage state. By repeating this protocol many times and accumulating statistics of random supercurrent switching events (as previously successfully implemented in various mesoscopic proximity circuits, e.g., nanowires and graphene layers [52,53]), one expects to reveal a bimodal distribution indicating the two parity states. If the separation of the two peaks in this distribution is wide enough, one can detect (with some fidelity) the parity state. Mutiterminal devices considered in this work can provide an actual hardware platform to conduct such experiments, and our transport theory will be useful in modeling future measurements. In particular, knowledge of the current-phase relationship is needed for determining the energy barrier of a phase slip that triggers the switching. Furthermore, these developments are also inspired by the potential application of multiterminal devices in the design of protected superconducting qubits.

ACKNOWLEDGMENTS

We would like to thank D. Van Harlingen for the discussions, especially on the topic of the gate dependence of the critical current fluctuations in topological Josephson junctions [21] and the feasibility of switching current experiments in the trijunction configuration. The work of H.-Y.X. was supported by National Science Foundation Grants No. DMR-1653661 and No. DMR-1743986. The work of A.L. was supported in part by the U.S. Department of Energy, Office of Science, Basic Energy Sciences, under Award No. DESC0017888, and the Army Research Office, Laboratories for Physical Sciences Grant No. W911NF-18-1-0115. H.-Y.X. acknowledges the hospitality of the Kavli Institute of Theoretical Sciences (KITS), where this work was partially done.

^[1] B. L. Al'tshuler, Fluctuations in the extrinsic conductivity of disordered conductors, Pis'ma Zh. Eksp. Theor. Fiz. **41**, 530 (1985) [JETP Lett. **41**, 648 (1985)].

^[2] B. L. Al'tshuler and D. E. Khmel'nitskii, Fluctuation properties of small conductors, Pis'ma Zh. Eksp. Theor. Fiz. 42, 291 (1985) [JETP Lett. 42, 359 (1986)].

^[3] P. A. Lee and A. D. Stone, Universal Conductance Fluctuations in Metals, Phys. Rev. Lett. 55, 1622 (1985).

^[4] P. A. Lee, A. D. Stone, and H. Fukuyama, Universal conductance fluctuations in metals: Effects of finite temperature, interactions, and magnetic field, Phys. Rev. B 35, 1039 (1987).

^[5] I. L. Aleiner and Y. M. Blanter, Inelastic scattering time for conductance fluctuations, Phys. Rev. B 65, 115317 (2002).

^[6] F. J. Dyson, Statistical Theory of the Energy Levels of Complex Systems, J. Math. Phys. 3, 140 (1962).

- [7] B. L. Altshuler and B. I. Shklovskii, Repulsion of energy levels and conductivity of small metal samples, Zh. Eksp. Theor. Fiz. 91, 220 (1986) [Sov. Phys. JETP 64, 127 (1986)].
- [8] M. L. Mehta, Random Matrices (Elsevier, Amsterdam, 2004).
- [9] S. G. den Hartog, C. M. A. Kapteyn, B. J. van Wees, T. M. Klapwijk, W. van der Graaf, and G. Borghs, Sample-Specific Conductance Fluctuations Modulated by the Superconducting Phase, Phys. Rev. Lett. 76, 4592 (1996).
- [10] K. Hecker, H. Hegger, A. Altland, and K. Fiegle, Conductance Fluctuations in Mesoscopic Normal-Metal/Superconductor Samples, Phys. Rev. Lett. 79, 1547 (1997).
- [11] P. W. Brouwer, On the random-matrix theory of quantum transport, Ph.D. thesis, Leiden University, 1997.
- [12] C. W. J. Beenakker, Random-matrix theory of quantum transport, Rev. Mod. Phys. 69, 731 (1997).
- [13] B. L. Al'tshuler and B. Z. Spivak, Mesoscopic fluctuations in a superconductor-normal metal-superconductor junction, Zh. Eksp. Theor. Fiz. 92, 609 (1987) [Sov. Phys. JETP 65, 343 (1987)].
- [14] C. W. J. Beenakker, Universal Limit of Critical-Current Fluctuations in Mesoscopic Josephson Junctions, Phys. Rev. Lett. 67, 3836 (1991).
- [15] J. T. Chalker and A. M. S. Macêdo, Complete Characterization of Universal Fluctuations in Quasi-One-Dimensional Mesoscopic Conductors, Phys. Rev. Lett. 71, 3693 (1993).
- [16] B. Sacepe, J. B. Oostinga, J. Li, A. Ubaldini, N. J. G. Couto, E. Giannini, and A. F. Morpurgo, Gate-tuned normal and superconducting transport at the surface of a topological insulator, Nat. Commun. 2, 575 (2011).
- [17] M. Veldhorst, M. Snelder, M. Hoek, T. Gang, V. K. Guduru, X. L. Wang, U. Zeitler, W. G. Van der wiel, A. A. Golubov, H. Hilgenkamp, and A. Bririkman, Josephson supercurrent through a topological insulator surface state, Nat. Mater. 11, 417 (2012).
- [18] J. R. Williams, A. J. Bestwick, P. Gallagher, S. S. Hong, Y. Cui, A. S. Bleich, J. G. Analytis, I. R. Fisher, and D. Goldhaber-Gordon, Unconventional Josephson Effect in Hybrid Superconductor-Topological Insulator Devices, Phys. Rev. Lett. 109, 056803 (2012).
- [19] S. Cho, B. Dellabetta, A. Yang, J. Schneeloch, Z. Xu, T. Valla, G. Gu, M. J. Gilbert, and N. Mason, Symmetry protected Josephson supercurrents in three-dimensional topological insulators, Nat. Commun. 4, 1689 (2013).
- [20] A. D. K. Finck, C. Kurter, Y. S. Hor, and D. J. Van Harlingen, Phase Coherence and Andreev Reflection in Topological Insulator Devices, Phys. Rev. X 4, 041022 (2014).
- [21] C. Kurter, A. D. K. Finck, P. Ghaemi, Y. S. Hor, and D. J. Van Harlingen, Dynamical gate-tunable supercurrents in topological Josephson junctions, Phys. Rev. B 90, 014501 (2014).
- [22] C. Kurter, A. D. K. Finck, Y. S. Hor, and D. J. Van Harlingen, Evidence for an anomalous current-phase relation in topological insulator Josephson junctions, Nat. Commun. 6, 7130 (2015).
- [23] I. Sochnikov, L. Maier, C. A. Watson, J. R. Kirtley, C. Gould, G. Tkachov, E. M. Hankiewicz, C. Brüne, H. Buhmann, L. W. Molenkamp, and K. A. Moler, Nonsinusoidal Current-Phase Relationship in Josephson Junctions from the 3D Topological Insulator HgTe, Phys. Rev. Lett. 114, 066801 (2015).
- [24] M. P. Stehno, V. Orlyanchik, C. D. Nugroho, P. Ghaemi, M. Brahlek, N. Koirala, S. Oh, and D. J. Van Harlingen, Signature

- of a topological phase transition in the Josephson supercurrent through a topological insulator, Phys. Rev. B **93**, 035307 (2016).
- [25] V. Mourik, K. Zuo, S. M. Frolov, S. R. Plissard, E. P. A. M. Bakkers, and L. P. Kouwenhoven, Signatures of Majorana fermions in hybrid superconductor-semiconductor nanowire devices, Science 336, 1003 (2012).
- [26] A. Das, Y. Ronen, Y. Most, Y. Oreg, M. Heiblum, and H. Shtrikman, Evidence of Majorana fermions in an Al-InAs nanowire topological superconductor, Nat. Phys. 8, 887 (2012).
- [27] D. Sherman, J. S. Yodh, S. M. Albrecht, J. Nygard, P. Krogstrup, and C. M. Marcus, Hybrid Double Quantum Dots: Normal, Superconducting, and Topological Regimes, Nat. Nanotechnol. 12, 212 (2017).
- [28] E. M. Spanton, M. Deng, S. Vaitiekenas, P. Krogstrup, J. Nygard, C. M. Marcus, and K. A. Moler, Current-phase relations of few-mode InAs nanowire Josephson junctions, Nat. Phys. 13, 1177 (2017).
- [29] R. M. Lutchyn, E. P. A. M. Bakkers, L. P. Kouwenhoven, P. Krogstrup, C. M. Marcus, and Y. Oreg, Realizing Majorana zero modes in superconductor-semiconductor heterostructures, Nat. Rev. Mater. 3, 52 (2018).
- [30] C. W. J. Beenakker, Random-matrix theory of Majorana fermions and topological superconductors, Rev. Mod. Phys. 87, 1037 (2015).
- [31] R.-P. Riwar, M. Houzet, J. S. Meyer, and Y. V. Nazarov, Multi-terminal Josephson junctions as topological matter, Nat. Commun. 7, 11167 (2016).
- [32] E. Eriksson, R.-P. Riwar, M. Houzet, J. S. Meyer, and Y. V. Nazarov, Topological transconductance quantization in a four-terminal Josephson junction, Phys. Rev. B 95, 075417 (2017).
- [33] J. S. Meyer and M. Houzet, Non-Trivial Chern Numbers in Three-Terminal Josephson Junctions, Phys. Rev. Lett. 119, 136807 (2017).
- [34] H.-Y. Xie, M. G. Vavilov, and A. Levchenko, Topological Andreev bands in three-terminal Josephson junctions, Phys. Rev. B 96, 161406(R) (2017).
- [35] H.-Y. Xie, M. G. Vavilov, and A. Levchenko, Weyl nodes in Andreev spectra of multiterminal Josephson junctions: Chern numbers, conductances, and supercurrents, Phys. Rev. B 97, 035443 (2018).
- [36] Z. Qi, H.-Y. Xie, J. Shabani, V. E. Manucharyan, A. Levchenko, and M. G. Vavilov, Controlled-Z gate for transmon qubits coupled by semiconductor junctions, Phys. Rev. B 97, 134518 (2018).
- [37] J. Erdmanis, A. Lukacs, and Y. V. Nazarov, Weyl disks: Theoretical prediction, Phys. Rev. B **98**, 241105(R) (2018).
- [38] O. Deb, K. Sengupta, and D. Sen, Josephson junctions of multiple superconducting wires, Phys. Rev. B **97**, 174518 (2018).
- [39] M. Houzet and J. S. Meyer, Majorana-Weyl crossings in topological multi-terminal junctions, arXiv:1810.09962.
- [40] E. Strambini, S. D'Ambrosio, F. Vischi, F. S. Bergeret, Y. V. Nazarov, and F. Giazotto, The ω -SQUIPT as a tool to phase-engineer Josephson topological materials, Nat. Nanotechnol. **11**, 1055 (2016).
- [41] Y. Cohen, Y. Ronen, J.-H. Kang, M. Heiblum, D. Feinberg, R. Melin, and H. Shtrikman, Non-local supercurrent of quartets in a three-terminal josephson junction, Proc. Natl. Acad. Sci. U.S.A. 115, 6991 (2018).
- [42] A. W. Draelos, M.-T. Wei, A. Seredinski, H. Li, Y. Mehta, K. Watanabe, T. Taniguchi, I. V. Borzenets, F. Amet, and

- G. Finkelstein, Supercurrent flow in multi-terminal graphene Josephson junctions, arXiv:1810.11632.
- [43] N. Pankratova, H. Lee, R. Kuzmin, M. Vavilov, K. Wickramasinghe, W. Mayer, J. Yuan, J. Shabani, and V. E. Manucharyan, The multi-terminal Josephson effect, arXiv:1812.06017.
- [44] G. Graziano, M. Pendharkar, J. S. Lee, C. Palmstrm, and V. S. Pribiag (private communication).
- [45] H.-J. Kwon, K. Sengupta, and V. M. Yakovenko, Fractional ac Josephson effects in p- and d-wave superconductors, Eur. Phys. J. B 37, 349 (2004).
- [46] P. Dita, Parametrisation of unitary matrices, J. Phys. A 15, 3465 (1982).
- [47] H. U. Baranger and P. A. Mello, Mesoscopic Transport through Chaotic Cavities: A Random *S*-Matrix Theory Approach, Phys. Rev. Lett. **73**, 142 (1994).
- [48] R. A. Jalabert, J.-L. Pichard, and C. W. J. Beenakker, Universal Quantum Signatures of Chaos in Ballistic Transport, Europhys. Lett. 27, 255 (1994).

- [49] R. Blumel and U. Smilansky, Classical Irregular Scattering and Its Quantum-Mechanical Implications, Phys. Rev. Lett. 60, 477 (1988).
- [50] C. M. Whisler, M. G. Vavilov, and A. Levchenko, Josephson currents in chaotic quantum dots, Phys. Rev. B 97, 224515 (2018).
- [51] P. A. Ioselevich, P. M. Ostrovsky, and M. V. Feigel'man, Josephson current between topological and conventional superconductors, Phys. Rev. B 93, 125435 (2016).
- [52] U. C. Coskun, M. Brenner, T. Hymel, V. Vakaryuk, A. Levchenko, and A. Bezryadin, Distribution of Supercurrent Switching in Graphene under the Proximity Effect, Phys. Rev. Lett. 108, 097003 (2012).
- [53] A. Murphy, P. Weinberg, T. Aref, U. C. Coskun, V. Vakaryuk, A. Levchenko, and A. Bezryadin, Universal Features of Counting Statistics of Thermal and Quantum Phase Slips in Nanosize Superconducting Circuits, Phys. Rev. Lett. 110, 247001 (2013).